Modelling punching shear failure under eccentric loading by means of nonlinear joint elements

Chunrong Lu[1], Robert L. Vollum[2] and Lorenzo Macorini[3]

[1]Department of Civil and Environmental Engineering, Imperial College London, United Kingdom, chunrong.lu18@imperial.ac.uk

[2]Department of Civil and Environmental Engineering, Imperial College London, United Kingdom, r.vollum@imperial.ac.uk

[3]Department of Civil and Environmental Engineering, Imperial College London, United Kingdom, l.macorini@imperial.ac.uk

Abstract

Flat slabs can fail in either flexure or punching shear. Punching failure is undesirable since it occurs suddenly without warning and can lead to progressive collapse. The paper describes a novel Joint shell Punching Model (JSPM), which models punching shear failure by combining nonlinear joint elements with reinforced concrete (RC) shell elements. The joint shear resistance is determined using the Critical Shear crack Theory as implemented in the next generation of Eurocode 2. The novelty of the approach is that the softening response of the joints is related to the joint shear displacement rather than the relative slab-column rotation as done in the classic JSPM. The method is validated for a series of test specimens from the literature. The proposed method is intended for modelling punching shear failure in whole building models subject to gravity and lateral loading.

1 Introduction

Reinforced concrete (RC) flat slabs are widely used in the construction industry due to their ease of construction and architectural flexibility. The thickness of flat slabs is typically governed by either deflection or punching shear. The latter occurs due to the concentration of shear forces around supporting columns and is particularly undesirable as it occurs abruptly and can lead to progressive collapse. Traditional nonlinear finite element analysis (NLFEA) with 3D solid elements provides the most accurate simulation of punching shear failure [1]-[3]. However, this approach is computationally expensive and impractical for modelling punching failure in entire buildings [4]. To address these limitations, Setiawan et al. [4] and Abu-Salma et al. [5] developed a Joint Shell Punching Model (JSPM) [6] in which punching shear failure is modelled with nonlinear joint elements inserted between nonlinear shell elements located around the punching control perimeter.

The classic JSPM calculates the joint shear resistance in terms of the relative slab-column rotation using the Critical Shear Crack Theory (CSCT) [7]. Like the classic CSCT, this approach does not capture the abrupt nature of punching shear failure since the joint shear resistance reduces gradually with increasing rotation. To address this limitation, the revised formulation of the JSPM proposed in this paper (depicted JSPMdisp) relates the joint shear resistance directly to the joint shear displacement. An advantage of this approach is that it avoids the need to trigger global punching failure prior to all joints failing, as done in [5]-[6] through the selection of a critical mid-side joint. The proposed enhancement enables direct computation of the peak load, unlike the classic JSPM [4]-[6], where post processing is required to determine the load at which the critical mid-side joint fails.

In the proposed formulation, the joint shear resistance model is calculated with the next generation of Eurocode 2 (EC2-23) [8]which determines punching resistance using a closed-form formulation of the CSCT [9]. As allowed by EC2-23, the proposed model (JSPMdisp) directly accounts for shear redistribution around the control perimeter following initial joint failure. The degree of shear redistribution is controlled through the adopted joint failure criterion. The paper presents the development and validation of JSPMdisp. The model is validated using experimental data from internal and external slab

column connections tested under both concentric and eccentric loading. Future research will extend this approach to the modelling punching failure under seismic loading.

2 Proposed Methodology

2.1 General overview

The proposed JSPMdisp offers greater computational efficiency than nonlinear finite element analysis (NLFEA) using 3D solid elements. As in the JSPM, joint elements are positioned within the slab around a control perimeter positioned at half the slab effective depth (d/2) from the column face.

2.2 Critical Shear Crack Theory (CSCT) and Eurocode 2 (EC2-23)

The JSPMdisp determines joint shear resistance using the closed form version of the CSCT implemented in EC2-23. The classic CSCT [7] relates punching resistance to the width of the critical shear crack which is assumed to depend on the slab rotation relative to the support. The slab rotation (Ψ) can be computed using NLFEA, as in the JSPM, or analytically following the approach of Kinnunen & Nylander [10], in which the slab is modelled as axisymmetric within the line of radial contraflexure. This approach simplifies kinematic assumptions for calculating the slab rotation Ψ. Following Muttoni & Schwartz [11] the width of the critical shear crack is assumed to be proportional to the product of the slab rotation Ψ and the slab effective depth d. The shear resistance depends on the width of the critical shear crack as well as the crack roughness which is a function of the coarse aggregate size. In the classic CSCT, the shear resistance is found graphically by determining the intersection point of the load-rotation and resistance-rotation functions. In the closed form version of the CSCT [9], the failure criterion is reformulated as a power-law enabling the failure load to be determined analytically. The resulting shear resistance is expressed in EC2-23 as follows:

$$\tau_{Rd} = \frac{0.6}{\gamma_V} \cdot k_{pb} \left(100\rho_l \cdot f_{ck} \cdot \frac{d_{dg}}{d_v}\right)^{\frac{1}{3}} \leq \frac{0.5}{\gamma_V} \cdot \sqrt{f_{ck}} \quad (1)$$

where

$$\rho_l = \sqrt{\rho_{l,x} \cdot \rho_{l,y}} \quad (2)$$

$$1 \leq k_{pb} = 3.6 \sqrt{1 - \frac{b_0}{b_{0.5}}} \leq 2.5 \quad (3)$$

in which $\boldsymbol{\rho_{l,x}, \rho_{l,y}}$ are the reinforcement ratios in the x and y directions, $\boldsymbol{b_0}$ is the column perimeter and $\boldsymbol{b_{0.5}}$ is the length of the control perimeter at $0.5\boldsymbol{d_v}$ from the column face. $\boldsymbol{d_{dg}}$ represents the crack roughness and equals 16 + d_g where d_g is the maximum aggregate size for $\boldsymbol{f_{ck} \leq 60\ MPa}$. In this paper, $\boldsymbol{\gamma_V = 1.0}$.

2.3 Implementation in ADAPTIC and Joint Elements

The proposed methodology is implemented in the nonlinear structural analysis software ADAPTIC [12], in which the slab is modelled with layered-shell elements based on the conventional Reissner-Mindlin hypothesis. The column is modelled as a line element connected to the slab with rigid links. Unlike the JSPM, the joint shear resistance is calculated in advance of the analysis using EC2-23. No reductions are made for loading eccentricity since this is accounted for in the NLFEA. The load-displacement response of the joints is using a trilinear symmetric elasto-plastic curve (smtr) [12] as illustrated in Fig. 3. Similarly to the JSPM, jel3 joint elements [12] are evenly spaced around a control perimeter positioned at d/2 from the column face. The jel3 elements, which have six degrees of freedom, are used to simulate punching shear failure.

Vertical separation of nodes 1 and 2 in Fig. 1 represents the shear deformation of the joint from its initial undeformed configuration. As shown in Fig. 2, node 3 is positioned in the slab, near the line of radial contraflexure, and node 4 is positioned on column chord above the slab. In the classic JSPM, the relative slab column rotation is calculated as the difference in the rotations at nodes 3 and 4. In the JSPMdisp, this is unnecessary since the joint strength calculated with equation (1) is independent of rotation. Following initial failure, the joint shear resistance softens as shown in Fig. 3. In eccentrically loaded connections, the peak load and softening branch are dependent on the choice of the stiffnesses

k_1 and k_2 in Fig. 3 as well as the shear displacement d_1. The choice of these coefficients determines the degree of load redistribution between joint elements following initial joint failure. The initial out-of-plane joint stiffness (k_0) is obtained using Eq. (4) from [4], in which l_{si} is the joint spacing, while the torsional resistance of the joints, T_{cri}, is determined using the approach of Abu-Salma et al. [5] which is based on the recommendations of Hsu [13].

$$k_0 = k_{red}\frac{E_c}{2(1+v)}l_{si} \quad (SI\ unit: N, mm) \tag{4}$$

in which k_{red} is an out-of-plane stiffness reduction factor which is taken as 1.0 in this paper unless noted otherwise.

$$T_{cri} = 0.217 l_{si}(h^2 + 6450)\sqrt[3]{f_c} \tag{5}$$

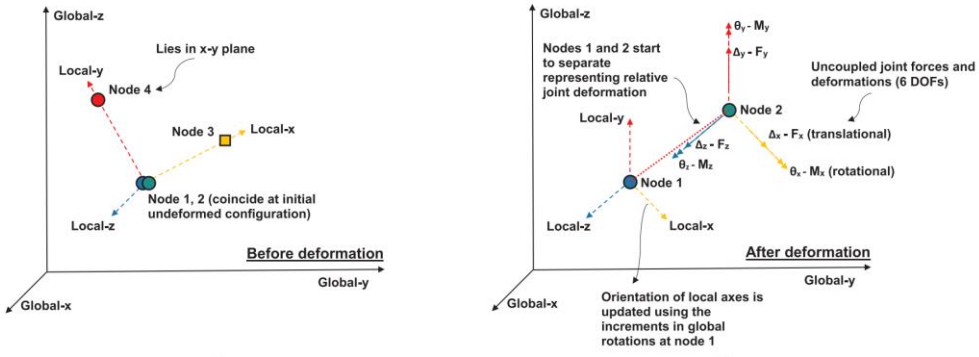


Fig. 1 Configuration, local force and deformation components of joint element (jel3): (left) before and (right) after deformation [4]

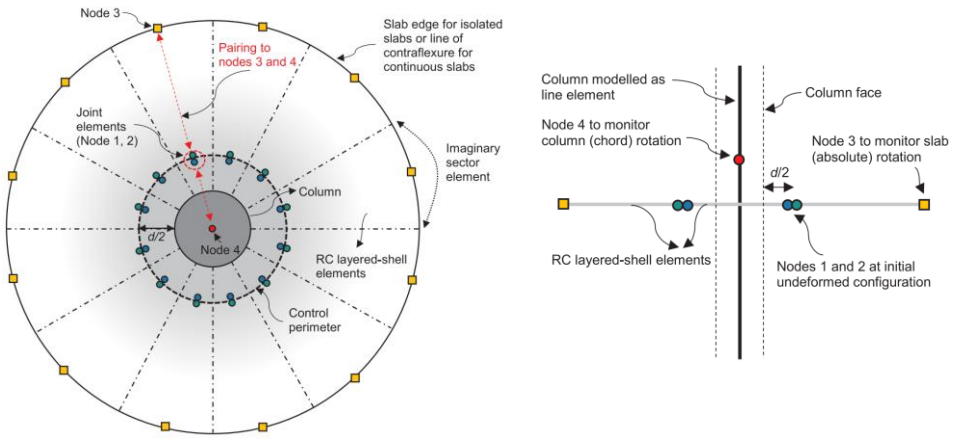


Fig. 2 Illustration of JSPM methodology [4]

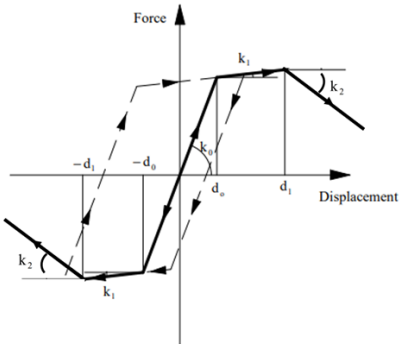


Fig. 3 Force-displacement curve of Trilinear symmetric elasto-plastic curve type in ADAPTIC [12]

3 Model Validation

3.1 Validation with JSPMdisp with test data and test result

The JSPMdisp is validated in this section by modelling several representative internal and edge punching shear specimens from the literature. The modelled internal column specimens are PT22 from Sagaseta et al. [14] and slab PD4 from Drakatos et al. [15]. The edge column specimens are XXX and HXXX from El-Salakawy et al [16]. Slab PT22 measured 3000×3000×250 mm^3 and was centrally supported on a 260×260 mm^2 column. It was concentrically loaded at eight points positioned on a radius of 1500 mm from the slab centre. Due to symmetry, a quarter model was modelled, as illustrated in Fig. 4. Specimens XXX and HXXX measured 1540×1020×120 mm^3 on plan and were supported by a 250×250 mm^2 column at the centre of the slab free edge. The remaining slab edges were simply supported. The column ends were loaded vertically and horizontally to maintain constant inward eccentricities relative to the column centreline of 300 mm in XXX and 660 mm in HXXX. Specimen PD4 measured 3000×3000×250 mm^3 on plan and was supported by a 390×390 mm^2 column at the centre of the slab. The slab edges were free. The gravity load was applied to PD4 at eight points positioned on a radius of 1500 mm from the slab centre. A pair of steel arms were used to introduce unbalanced moment as shown in Fig. 4. The distance between the loading points at the ends of the steel arms is 7.2 m simulating a prototype structure with the same span.

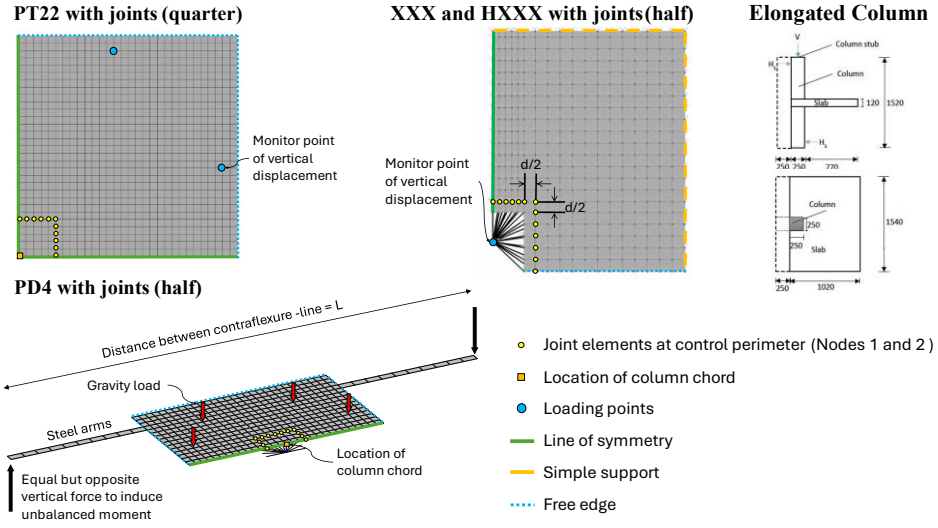


Fig. 4 Quarter model of PT22, half model of XXX and HXXX, and half model of PD4

All analyses were initially conducted using static analysis with the arc-length method, as used in previous studies with the JSPM and JSPME. The analysis began with force control, as the arc-length method cannot be applied in the initial phase in ADAPTIC. When the softening branch could not be successfully obtained, displacement control was employed to capture the softening response. If the softening branch still could not be determined, a dynamic analysis using the line search method was adopted.

3.2 Influence of d_1 and k_2

Fig. 5 compares the experimental load-displacement responses of the modelled slabs with numerical results obtained using the JSPMdisp, the original JSPM [4] for internal columns, and the JSPME [5] for edge columns. JSPMdisp was calibrated by systematically varying k_2 and d_1 (see Fig. 3) as illustrated in Figs. 5 and 6. The displacement d_0 is found by dividing the joint shear resistance by the stiffness parameter k_0 (see Eq. (4)) while k_1 was taken as 0 throughout. Fig. 5 shows the influence of varying the plateau length ($\Delta d_1=d_1-d_0$). Varying k_2 and d_1 has no influence on the failure load of PT22 since it was concentrically loaded. However, the load displacement response is affected as shown in Fig. 5. The failure load of eccentrically loaded specimens is affected by varying k_2 and d_1, as illustrated in Fig. 6, since these parameters control the redistribution of shear force from failing to non-failing joints. Fig. 6 shows that reducing k_2 results in a more gradual unloading response. For specimens subjected to complex loading conditions, such as XXX and PD4, a smaller k_2 facilitates the formation of a softening branch by extending the duration of joint softening, as discussed in Section 4.

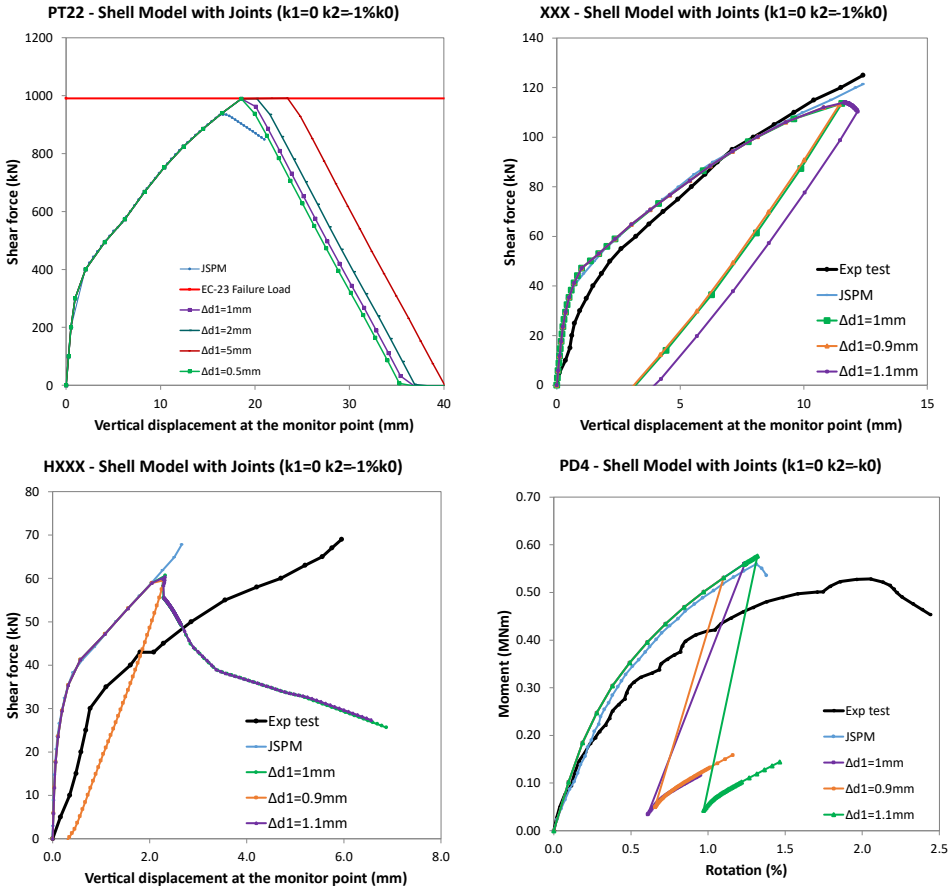


Fig. 5 Influence of plateau distance Δd1 on the load-displacement response of PT22 (Internal column), XXX (edge column, e=300 mm), HXXX (edge column, e=660 mm), and PD4 (eccentrically loaded internal column specimen)

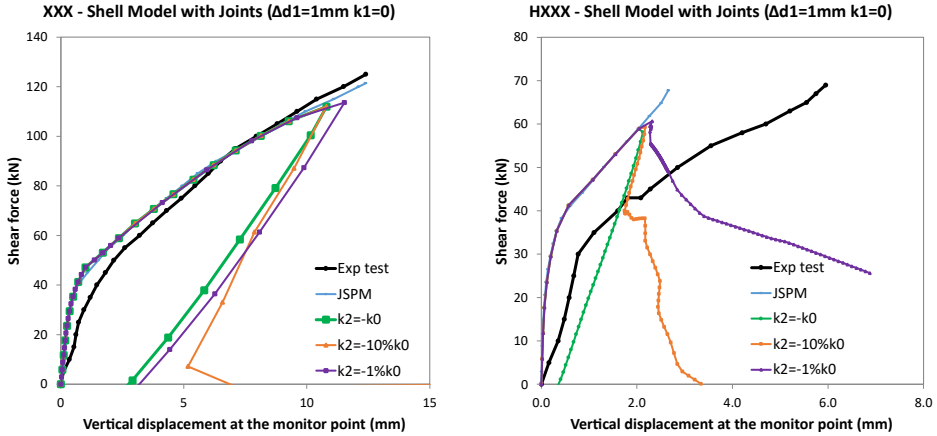


Fig. 6 Influence of the gradient of the softening strength k_2 of selected slabs: Internal slab: PT22, PL5 and PL10; Edge slab: XXX (e=300 mm) and HXXX (e=660 mm); Internal slab: PD4 under monotonic load

4 Analysis and discussion

4.1 Shear distribution around control perimeter

Figs. 7-9 illustrate the distribution of joint shear force utilisation around the punching control perimeter for XXX, and PD4. Fig. 7 shows the sequence of plotting joint elements along the control perimeter for each specimen. Fig. 8 shows the influence on joint shear force utilisation in XXX of taking: $k_2 = -k_0$, $k_2 = -1\%\ k_0$ and $k_2 = -10\%\ k_0$. In all three cases, the plateau of the joint shear force-displacement relationship is flat ($k_1 = 0$) and of length (Δd_1) 1 mm. A softening branch developed for each case. The output order follows the sequence of load application on the specimen. In Fig. 8, P_u depicts the failure load, while outputs recorded after the peak shear force output correspond to the global softening branch.

For $k_2 = -k_0$ and $k_2 = -10\%\ k_0$, the joint elements near the slab free edge do not reach their maximum resistance at the failure load. However, for $k_2 = -1\%\ k_0$, the joint elements near the free edge do reach their resistance at the failure load. Comparing the three cases, it is observed that a smaller k_2 enables greater shear force redistribution, increasing the likelihood of joint elements near the free edge reaching higher utilisation levels.

Fig. 9 presents the shear force distribution of PD4, an internal column punching specimen subjected to an unbalanced moment. It also compares the effects of different joint softening stiffness values when $\Delta d_1 = 1$ mm and $k_1 = 0$, specifically $k_2 = -1\%\ k_0$, $k_2 = -10\%\ k_0$, and $k_2 = -k_0$.

- $k_2 = -k_0$ successfully develops a global softening branch, as shown in Fig. 10.
- $k_2 = -10\%\ k_0$ reaches a stationary point first, as shown in Fig. 11, after which the moment increases as the rotation increases.
- $k_2 = -1\%\ k_0$ does not develop a global softening branch, but Fig. 9 shows how the shear force evolves throughout the steps until reaching the peak load.
- Here, M_u represents the peak moment achieved in the analysis.

In the $k_2 = -k_0$ case, the joint elements at the corner on the heavily loaded side reach their capacity first, as shown in Fig. 9, followed by the redistribution of shear force to the surrounding joints. In the model with softening branching ($k_2 = -k_0$ case), shear force further redistributes to the less loaded side as the global moment decreases.

The behaviour of $k_2 = -1\%\ k_0$ is similar to that of $k_2 = -k_0$, with joints on the heavily loaded side reaching their resistance when the peak global moment is attained.

However, for the $k_2 = -10\%\ k_0$ case, the corner joints on the less loaded side reach their resistance at M_u. The contribution of each lateral resisting mechanism is discussed in Section 4.2.

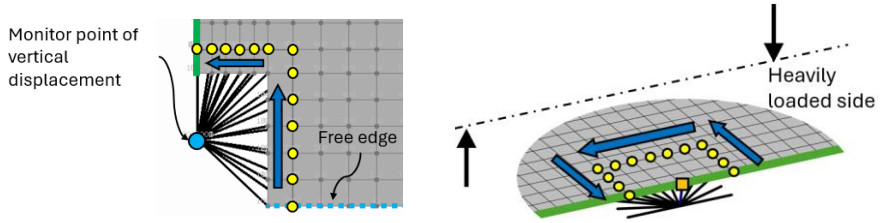
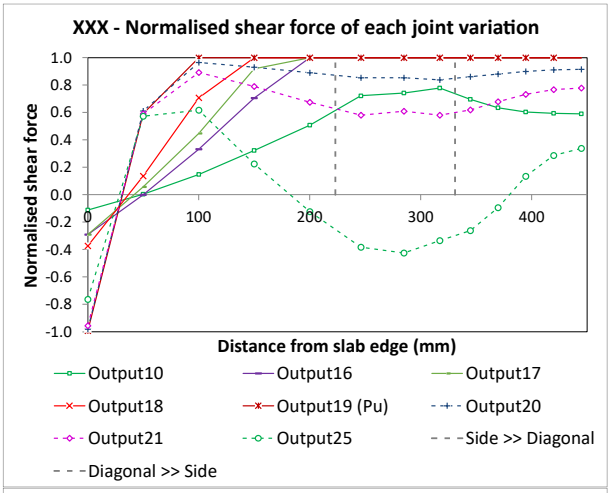
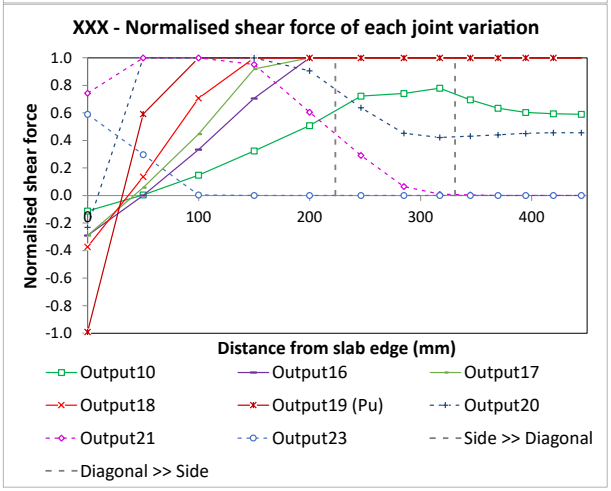


Fig. 7 Location of joint elements along the control perimeter of XXX (left) and PD4 (right)



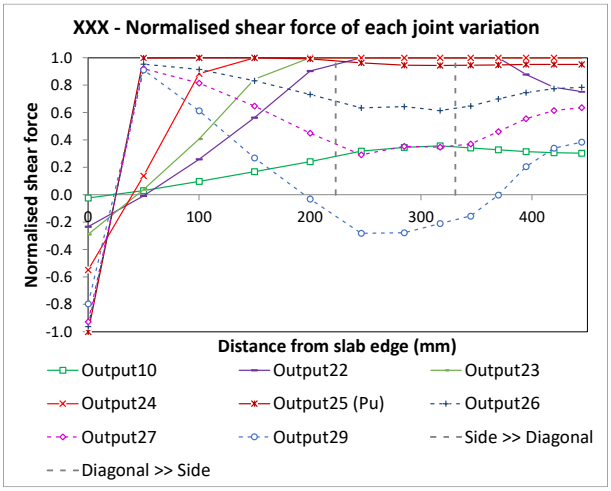
Δd_1=1mm k_1=0 k_2=-k_0

Output	Shear force (kN)	P/Pu
10	58.94	0.526
16	94.30	0.842
17	100.19	0.895
18	106.09	0.947
19	111.98 (Pu)	1.000
20	100.45	0.897
21	79.12	0.707
25	1.52	0.014



Δd_1=1mm k_1=0 k_2=-10%k_0

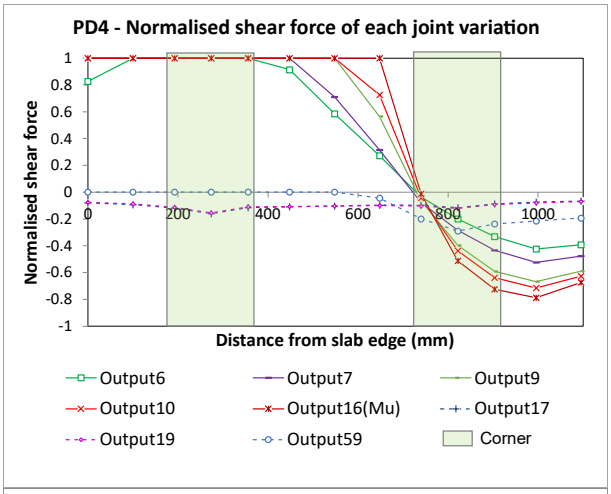
Output	Shear force (kN)	P/Pu
10	58.94	0.526
16	94.30	0.842
17	100.19	0.895
18	106.09	0.947
19	111.98 (Pu)	1.000
20	87.06	0.777
21	61.33	0.548
23	7.17	0.064



Δd_1=1mm k_1=0 k_2=-1%k_0

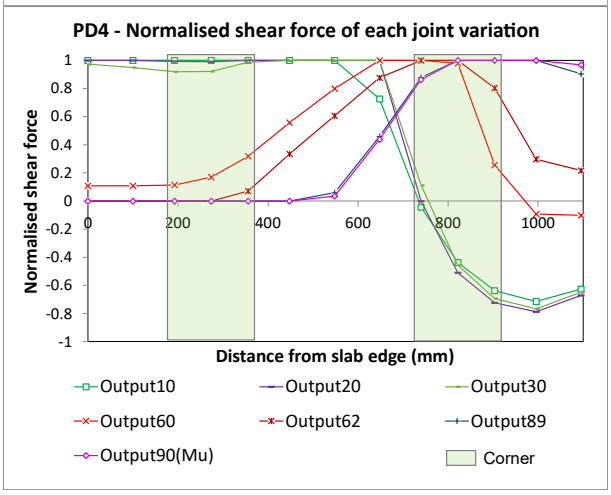
Output	Shear force (kN)	P/Pu
10	29.47	0.259
22	86.46	0.761
23	98.12	0.864
24	107.43	0.946
25	113.62 (Pu)	1.000
26	87.32	0.769
27	61.37	0.540
29	14.01	0.123

Fig. 8 Shear force utilisation of each joint of XXX around control perimeter – with various k_2



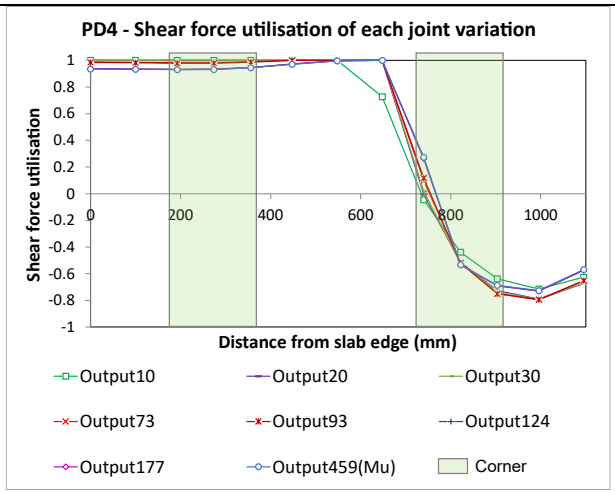
Δd_1=1mm k_1=0 k_2=-k_0

Output	Moment (MNm)	M/Mu
6	0.352	0.629
7	0.396	0.705
9	0.469	0.837
10	0.501	0.894
16	0.561 (Mu)	1.000
17	0.034	0.061
19	0.036	0.065
59	0.117	0.208



Δd_1=1mm k_1=0 k_2=-10%k_0

Output	Moment (MN.m)	M/Mu
10	0.501	0.660
20	0.564	0.743
30	0.576	0.759
60	0.587	0.773
62	0.596	0.785
89	0.754	0.994
90	0.759 (Mu)	1.000



Δd_1=1mm k_1=0 k_2=-1%k_0

Output	Moment (MN.m)	M/Mu
10	0.501	0.433
20	0.564	0.487
30	0.578	0.499
73	0.704	0.608
93	0.800	0.691
124	0.901	0.778
177	1.001	0.864
459	1.158 (Mu)	1.000

Fig. 9 Shear force utilisation of each joint of PD4 around control perimeter – with various k_2

4.2 Contribution of each moment resisting mechanism

Fig. 10 illustrates the contribution of each moment resisting mechanism for specimen PD4 with Δd_1 = 1 mm, $k_1 = 0$, and $k_2 = -k_0$. As shown in Figs. 5, 6 and 10 these parameters give reasonable estimates of the experimental failure loads for all the investigated specimens. Before failure (point A) at a slab-column rotation of 1.23%, the contributions of the resisting mechanisms increase in proportion to the applied moment. Just before failure, the proportion of the unbalanced moment caused by eccentric shear is reduced by approximately 10%. The overall moment-rotation response closely matches the experimental test results, with a measured resistance of 0.53 MNm in the test and a predicted value of 0.56 MNm. After failure (point A), the moment drops abruptly following which the results are no longer meaningful.

Fig. 10 shows that taking Δd_1=1mm k_1=0 k_2=-k_0 underestimates the rotation at failure of PD4. In an attempt, to increase the rotation at failure the slope of the softening branch k_2 was reduced to -10%k_0 as illustrated in Fig. 11 which also shows the contribution of each moment resisting mechanism for this case. When k_2 is reduced to -10%k_0, the unbalanced moment reaches a stationary point at approximately 0.6 MNm, after which the moment continues to increase. Referring to Fig. 9, these moments correspond to outputs around 62, at which shear force redistributes from the heavily loaded side to the adjacent joint elements on the less loaded side. At this point, the eccentric shear contribution decreases to zero, following which it gradually increases until the global moment reaches its peak. The overestimate of moment shown in Fig. 11 results from the transfer of moment through flexure and torsion being overestimated. Future work will focus on imposing suitable limits on these to better reflect the experimentally observed behaviour.

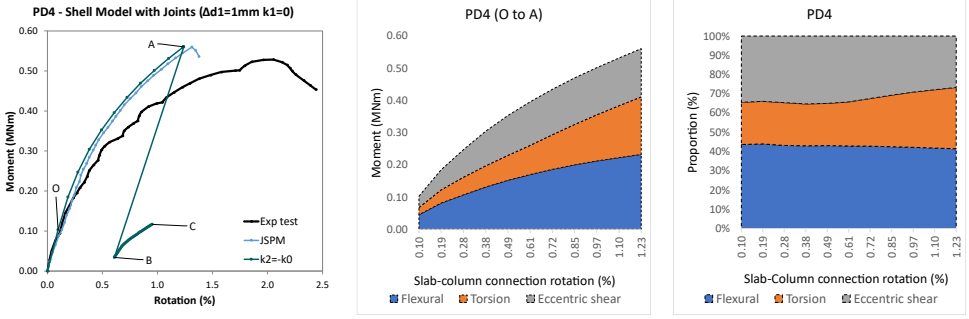


Fig. 10 Contribution of each lateral resisting mechanism in PD4 as a function of slab-column connection rotation (Δd_1=1mm k_1=0 k_2=-k_0)

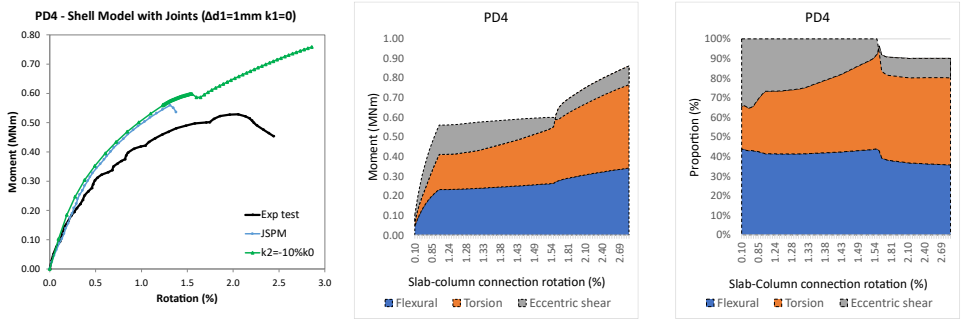


Fig. 11 Contribution of each lateral resisting mechanism in PD4 as a function of slab-column connection rotation (Δd_1=1mm k_1=0 k_2=-10%k_0)

5 Conclusion

The paper describes a novel Joint Shell Punching Model (depicted JSPMdisp) for simulating punching failure in flat slabs. The model is intended for modelling punching shear failure in whole building models subject to combined gravity and lateral loading.

The novelty of the JSPMdisp is that joint shear resistance is directly related to the joint shear displacement, rather than the relative slab-column rotation, as done in the classic JSPM [4]-[6]. Punching failure is modelled with joint elements which are distributed uniformly around a punching control perimeter located at 0.5d from the column face. The joint elements connect the shell elements to either side of the control perimeter. Currently, the peak joint shear resistance in the JSPMdisp is pre-determined using EC2-23. The joint shear-displacement response is defined using a trilinear elasto-plastic curve (see Fig. 3). The initial joint stiffness is taken as that previously used in the classic JSPM [4]. A sensitivity study was conducted to identify suitable values for the remaining parameters defining the joint response; the plastic plateau distance (Δd_1), the plateau gradient (k_1), and the softening stiffness (k_2). Based on comparison of model predictions with experimental data, suggested values are Δd_1 = 1 mm, k_1 = 0 and k_2 = -k_0.

References

[1] A. S. Genikomsou and M. A. Polak. 2015. "Finite element analysis of punching shear of concrete slabs using damaged plasticity model in ABAQUS." Eng. Struct., vol. 98, pp. 38–48. DOI: 10.1016/j.engstruct.2015.04.016.

[2] J. Shu et al. 2017. "Internal force distribution in RC slabs subjected to punching shear." Eng. Struct. vol. 153, pp. 766–781,. DOI: 10.1016/j.engstruct.2017.10.005.

[3] C. Y. M. Goh and T. D. Hrynyk. 2018. "Numerical Investigation of the Punching Resistance of Rein-forced Concrete Flat Plates." Journal of Structural Engineering (New York, N.Y.), vol. 144, (10), pp. 339–343. DOI: 10.1061/(ASCE)ST.1943-541X.0002142.

[4] A. Setiawan et al. 2019. "Efficient 3-D modelling of punching shear failure at slab-column connections by means of nonlinear joint elements." Eng. Struct., vol. 197, pp. 109372. Available: https://www.sciencedirect.com/science/article/pii/S0141029618330992. DOI: 10.1016/j.engstruct.2019.109372.

[5] D. Abu-Salma, R. Vollum, and L. Macorini. 2021. "Modelling punching shear failure at edge slab-column connections by means of nonlinear joint elements," vol. 34, pp. 630–652. Doi: 10.1016/j.istruc.2021.07.092.

[6] A. Setiawan et al. 2020. "Punching of RC slabs without transverse reinforcement supported on elongated columns." Structures, vol. 27, pp. 2048–2068. Available: https://dx.doi.org/10.1016/j.istruc.2020.08.017. DOI: 10.1016/j.istruc.2020.08.017.

[7] A. Muttoni. 2008. "Punching shear strength of reinforced concrete slabs without transverse reinforce-ment." ACI Structural Journal, vol. 105, (4), pp. 440–450.

[8] European Committee for Standardization (CEN), "Eurocode 2: Design of Concrete Structures – Part 1-1: General Rules and Rules for Buildings." 2023.

[9] A. Muttoni, M. Fernández Ruiz and J. T. Simões. 2018. "The theoretical principles of the critical shear crack theory for punching shear failures and derivation of consistent closed-form design expressions." Structural Concrete, vol. 19, (1), pp. 174–190. Available: https://doi.org/10.1002/suco.201700088. DOI: 10.1002/suco.201700088.

[10] S. Kinnunen and H. Nylander, Punching of Concrete Slabs without Shear Reinforcement. 1960Available: https://worldcat.org/title/19988711.

[11] A. Muttoni and J. Schwartz. 1991. "Behaviour of beams and punching in slabs without shear reinforce-ment." IABSE Reports = Rapports AIPC = IVBH Berichte, vol. 62, pp. 703. DOI: 10.5169/seals-47705.

[12] B. A. Izzuddin. 1991. "Nonlinear Dynamic Analysis of Framed Structures." Imperial College London (University of London). [Online]. Available: http://hdl.handle.net/10044/1/8080.

[13] T. T. C. Hsu. 1968. "Torsion of structural concrete: Behavior of reinforced concrete rectangular mem-bers." Available: https://api.semanticscholar.org/CorpusID:137948096.

[14] J. Sagaseta et al. 2011. "Non-axis-symmetrical punching shear around internal columns of RC slabs without transverse reinforcement." Magazine of Concrete Research, vol. 63, (6), pp. 441–457. Available: https://doi.org/10.1680/macr.10.00098. DOI: 10.1680/macr.10.00098.

[15] I. Drakatos. 2016. "Seismic Behaviour of Slab-Column Connections without Transverse Reinforcement." DOI:10.13140/RG.2.2.33267.84003.

[16] E. El-Salakawy, M. Polak and M. Soliman. 2011. "Slab-column edge connections subjected to high moments." Canadian Journal of Civil Engineering, vol. 25, pp. 526–538. DOI: 10.1139/cjce-25-3-526.